Published in final edited form as:

Stat Atlases Comput Models Heart. 2022 September ; 13593: 112–122.

doi:10.1007/978-3-031-23443-9_11.

An Atlas-Based Analysis of Biventricular Mechanics in Tetralogy of Fallot

Sachin Govil[1], **Sanjeet Hegde**[2], **James C. Perry**[2], **Jeffrey H. Omens**[1], **Andrew D. McCulloch**[1]

[1]Department of Bioengineering, University of California San Diego, San Diego, USA

[2]Division of Cardiology, Rady Children's Hospital San Diego, San Diego, USA

Abstract

The current study proposes an efficient strategy for exploiting the statistical power of cardiac atlases to investigate whether clinically significant variations in ventricular shape are sufficient to explain corresponding differences in ventricular wall motion directly, or if they are indirect markers of altered myocardial mechanical properties. This study was conducted in a cohort of patients with repaired tetralogy of Fallot (rTOF) that face long-term right ventricular (RV) and/or left ventricular (LV) dysfunction as a consequence of adverse remodeling. Features of biventricular end-diastolic (ED) shape associated with RV apical dilation, LV dilation, RV basal bulging, and LV conicity correlated with components of systolic wall motion (SWM) that contribute most to differences in global systolic function. A finite element analysis of systolic biventricular mechanics was employed to assess the effect of perturbations in these ED shape modes on corresponding components of SWM. Perturbations to ED shape modes and myocardial contractility explained observed variation in SWM to varying degrees. In some cases, shape markers were partial determinants of systolic function and, in other cases, they were indirect markers for altered myocardial mechanical properties. Patients with rTOF may benefit from an atlas-based analysis of biventricular mechanics to improve prognosis and gain mechanistic insight into underlying myocardial pathophysiology.

Keywords

Congenital heart disease; Biomechanics; Statistical atlases

1 Introduction

While shape, wall motion, and hemodynamics are important indicators of regional ventricular wall mechanics, they form an incomplete picture. Regional stresses and strains are more direct and sensitive indicators of regional myocardial mechanics because they are related *via* intrinsic myocardial material properties, such as active myofiber contractility and passive stiffness [1–3]. Several groups have demonstrated the feasibility of patient-specific biomechanical modeling [4, 5], though this depends on accurate measures of

sagovil@eng.ucsd.edu .

[6]Competing Interests

The rest of the authors do not have any conflict-of-interest.

myocardial anatomy, hemodynamics, activation patterns, and wall motion to identify unknown mechanical properties, and still requires material assumptions that cannot be measured *in vivo*. Patient-specific models of biomechanics are also highly nonlinear, and consequently, their solutions can significantly amplify measurement uncertainties.

The use of statistical shape modeling to characterize major features of ventricular shape and wall motion at the population-level has been insightful for better understanding many cardiac pathologies including several congenital heart diseases. By identifying major modes of variation in biventricular shape and wall motion in various patient cohorts, many groups have observed statistically significant relationships between ventricular shape modes and ventricular function or clinical outcomes [6–10]. These analyses, however, do not establish causal relationships between shape and function or outcomes. When statistical shape models are integrated with cardiac biomechanics models, however, mechanistic relationships between observable features of cardiac shape, function, and intrinsic myocardial mechanical properties can be tested further, which may be important for understanding and predicting ventricular remodeling. This is particularly relevant in patients with repaired tetralogy of Fallot (rTOF) that face long-term, adverse right ventricular (RV) and/or left ventricular (LV) remodeling as a consequence of surgical repair [11–14].

The current study proposes an efficient strategy for exploiting the statistical power of cardiac atlases to investigate the extent to which clinically significant variations in ventricular shape explain corresponding differences in ventricular function directly or whether they are indirect markers of altered myocardial mechanical properties. Patient-specific relationships between end-diastolic shape and systolic wall motion were assessed for consistency with properties representative of the cohort mean and, in the case of deviations, were explored for their ability to explain differences in clinical outcomes. Specifically, in a rTOF patient cohort, we tested the hypothesis that shape variations can be direct determinants of variations in systolic function, but may also be indirect markers of altered myocardial mechanical properties that could help stratify clinical outcomes in rTOF.

2 Methods

2.1 Study Population and Geometry Fitting

A previously identified cohort of 84 rTOF patients was employed in this study [15]. Cardiovascular magnetic resonance (CMR) images and associated clinical data for this cohort were retrospectively collected from the Cardiac Atlas Project database (https://www.cardiacatlas.org) [16]. Deidentified datasets were contributed from two clinical centers (Rady Children's Hospital, San Diego, CA, US and The Center for Advanced Magnetic Resonance Imaging, Auckland, NZ) with approval from local institutional review boards *via* waiver of informed consent (UCSD IRB 201138 and HDEC 16/STH/248, respectively). All patients underwent standard-of-care CMR examination, and CMR images were acquired using 1.5T MRI scanners, including Siemens Avanto (Siemens Medical Systems) and GE Discovery (GE Healthcare Systems), as described previously [15]. Three-dimensional, patient-specific geometric models were customized to a biventricular subdivision surface template mesh using manually drawn contours at end-diastole (ED) and end-systole (ES)

in Segment (Medviso) along with manually annotated anatomical landmarks, as described previously [15].

2.2 Atlas-Based Analysis of Systolic Wall Motion

A statistical atlas of systolic wall motion (SWM) was generated from the patient-specific geometric models at ED and ES. Patient-specific surface points at ED and ES were first aligned to population mean ED surface points by a rigid registration using a Procrustes alignment. A vector field of SWM was then computed between ED and ES for each patient. Principal component analysis (PCA) was then used to evaluate the distribution of SWM across the rTOF cohort.

2.3 Sensitivity of Biventricular Function to Systolic Wall Motion

The effects of the first ten SWM modes on LV and RV function were analyzed by varying individual modes and computing corresponding LV and RV ejection fractions (EFs). For each SWM mode, wall motion displacements were calculated for Z-scores between − 2 and 2 in steps of 0.5 and were added to the mean ED shape of the rTOF cohort to yield an ES shape. The mean ED model volumes and computed ES model volumes were used to calculate EFs for each score along each mode. The sensitivity of changes in LV and RV EF to changes along an individual SWM mode was then computed using linear regression.

2.4 Association of End-Diastolic Shape with Systolic Wall Motion

Associations between ED shape modes and SWM modes were assessed *via* univariate regression analysis. ED shape modes were taken from an ED shape atlas previously derived from the same cohort of rTOF patients [15]. ED shape modes that were previously found to be significantly associated with differences in prognosis were correlated with the five SWM modes that had the greatest effect on combined LV/RV function. ED shape modes that had significant correlations with systolic wall motion modes were perturbed in a finite element (FE) mechanics framework to assess the degree to which shape markers are direct determinants of systolic function.

2.5 Finite Element Analysis of Biventricular Biomechanics

Biomechanics simulations were performed using biventricular, cubic-Hermite FE meshes generated from the ED shape atlas. A compressible, nonlinearly elastic, transversely isotropic constitutive model was used to define the passive material properties of the myocardium in the fiber direction (a, a_f, b, b_f) [17, 18]. Mesh fiber directions were assigned using a rule-based approximation, where fibers were defined relative to the circumferential direction in the LV and RV epicardium as −60° and −25°, respectively, and in the LV and RV endocardium as 60° and 0°, respectively [19]. In order to define a physiologically realistic transmural gradient, fiber directions were linearly interpolated from epicardium to endocardium. Active contraction of the myocardium was governed by a transversely isotropic active tension model, where the transverse direction active force was specified to be 70% of the fiber direction active force. An unloaded, stress-free reference geometry for each simulation was approximated using a previously described iterative, inflation-deflation algorithm [5], with convergence criteria defined as a change in computed ED volumes

between successive iterations of less than 2%. Pressure boundary conditions were applied normal to the endocardial surfaces using average LV and RV ED and ES catheterization pressures from rTOF patients with available clinical data. The average LV and RV EDPs were 1.05 kPa and 0.95 kPa, respectively, and the average LV and RV ESPs were 11 kPa and 5.15 kPa, respectively. Additionally, nodal boundary conditions were implemented to constrain epicardial longitudinal and circumferential displacement at the valve planes.

Mean passive material properties were approximated by estimating the reference geometry for the mean ED shape. Material constants, b and b_f, were taken from previously reported values from human subjects with heart failure [5], while material constants, a and a_f, were estimated by altering these parameters until the FE-computed ED model volumes at mean ED pressure matched the atlas mean ED model volumes. The material anisotropy ratio of a to a_f was maintained so that only a single parameter was estimated. Mean active material properties were approximated by linearly increasing the active tension developed in the myocardium until the FE-computed ES model volumes at mean ES pressure matched the atlas mean ES model volumes. These mean passive and active material properties were then used in additional FE simulations with perturbations of ED geometry corresponding to Z-scores of ± 2 for tested ED shape modes. The computed ED and ES mesh geometries for each shape perturbation were sampled on the endocardial and epicardial surfaces in order to compute wall motion displacements, which were then projected onto the SWM atlas to compute Z-scores for corresponding SWM modes of interest. SWM mode Z-scores from FE-computed models were compared with those predicted from linear regression models fit to patient data. All FE analysis was performed in *Continuity 6* (https://www.continuity.ucsd.edu), a problem-solving environment for multiscale biomechanics and electrophysiology.

2.6 Statistical Analysis

Statistical analysis was carried out using the SciPy Python library (https://www.scipy.org). Statistical associations in the regression analysis are denoted by p-values with a significance level of 0.05. A Bonferroni correction was used to adjust the significance level to correct for multiple comparisons.

3 Results

3.1 Atlas of Systolic Wall Motion and Associations with End-Diastolic Shape

An atlas of SWM was constructed from a cohort of 84 rTOF patients. The first ten SWM modes explained approximately 70% of the variation in the study population (Fig. 1A), and their effects on LV and RV function were analyzed (Fig. 1B). ED shape modes that were previously found to be significantly associated with differences in prognosis in rTOF correlated with SWM modes that had the greatest effect on combined LV/RV function (Fig. 1C).

ED4, which is a specific marker of opposing RV apical dilation and LV dilation, was significantly correlated with SWM7, which appears to be a specific marker of displacement around the RV base, RV apex, and the entire LV free wall (Fig. 2A). ED6, which is a specific

marker of RV basal bulging and LV conicity, was significantly correlated with SWM8, which appears to be a specific marker of displacement around the posterior RV base, LV base, and LV apex (Fig. 2B). These ED shape modes were perturbed in a FE model to assess the degree to which shape differences are direct determinants of observed changes in SWM.

3.2 Finite Element Analysis of Biventricular Biomechanics

Parameterization of the material properties of the mean FE-computed model resulted in an average absolute error compared with the mean atlas model of 1.06 mm and 1.44 mm at ED and ES, respectively, both of which are within voxel resolution of the original CMR images used to make the patient-specific geometric models (0.6 – 1.75 mm). The estimated mean passive material properties are shown in Table 1, where the approximated stiffness of the RV was twice that of the LV. The mean peak active tension developed in the myocardium was estimated to be 164 kPa in both the LV and RV. A summary of global volume and functional measurements for the mean FE-computed model and atlas model are shown in Table 2. Overall, the FE-computed model measurements demonstrate good agreement with the atlas model measurements. Lastly, the resulting SWM Z-scores for the mean FE-computed model were compared to those for the mean atlas model, which are zero by definition, for the first five SWM modes (Fig. 3). Overall, the Z-score differences between the FE-computed model and atlas model are within an acceptable range.

FE simulations with perturbed ED shapes were executed with mean material properties, and their deformed ES shapes were computed (Fig. 4). The FE-computed change in LV and RVEF were −5.3% and −0.2%, respectively, along the shape change in ED4 and 3.2% and 3.1%, respectively, along the shape change in ED6. The predicted change in LV and RV EF, based on the correlations between ED shape and SWM and the observed effect on EF (Fig. 1), were −2.8% and −3.0%, respectively along the shape change in ED4 and −3.4% and −2.0%, respectively, along the shape change in ED6.

The SWM Z-scores for the FE-computed ED shape perturbations were computed and compared with those predicted from linear regression models fit to patient data. For the correlation between ED4 and SWM7 (Fig. 5A), the FE-computed slope was −0.12 compared to −0.32 in the patient data. For the correlation between ED6 and SWM8 (Fig. 5B), the FE-computed slope was 0.02 compared to −0.29 in the patient data.

For FE-computed models that did not match the predicted SWM, the model contractility was adjusted to produce a better match. For both ED4 and ED6, a more negative Z-score was associated with increased contractility (Fig. 6A and B, respectively).

4 Discussion

Patients with rTOF are at risk of developing RV and LV dysfunction as a consequence of adverse ventricular remodeling. While statistical shape modeling has been used to identify features of ventricular remodeling that are associated with function in the rTOF population, it was not clear whether shape features are direct determinants of systolic function. In this study, cardiac biomechanics models were integrated with statistical shape models to test whether clinically significant variations in ventricular shape explain corresponding

differences in systolic function or if they are indirect markers of altered myocardial mechanical properties, or both.

4.1 Shape Determinants of Biventricular Function

By correlation analysis, previously identified biventricular ED shape modes that had significant associations with differences in prognosis of patients with rTOF were also significantly correlated with the components of SWM that contributed most to differences in LV and RV EF. Specifically, greater RV apical dilation and less LV dilation were associated with greater systolic displacements near the RV base and apex and the entire LV free wall, and greater RV basal bulging and higher LV conicity were associated with greater systolic displacements around the posterior RV base and the LV base and apex. The mechanisms of these shape-function relationships were tested using FE models in which observed shape mode differences were simulated without changes in material properties or boundary conditions.

In the case of RV apical dilation and LV dilation, differences in the shape alone partially explained observed differences in systolic function. In terms of global functional metrics, less RV apical dilation and greater LV dilation accounted for more than the expected decrease in LV EF (−5.3% vs. −2.8%) but none of the expected decrease in RV EF (−0.2% vs. −3.0%). In terms of regional measures of SWM, differences in the shape alone explained 38% of the variation in wall motion. Assuming that the remaining correlation could be explained by differences in myocardial material properties, we observed that greater RV apical dilation and less LV dilation were associated with increased contractility. Therefore, greater RV apical dilation may be a surrogate for increased RV basal and apical contractility that may also serve as a compensatory mechanism to prevent LV dilation and preserve LV function. This mechanism may explain why patients with rTOF that had greater RV apical dilation and less LV dilation tended to have better prognoses [15].

In the case of RV basal bulging and LV conicity, differences in shape alone explained the opposite change in systolic function. In terms of global functional metrics, less RV basal bulging and lower LV conicity led to an increase in LV and RV EF (3.2% and 3.1%, respectively) rather than an expected decrease in LV and RV EF (−3.4% and −2.0%, respectively). In terms of regional measures of SWM, changing shape alone produced a slope that was the opposite sign as that of the regression model. When altering myocardial contractility to better match the ED shape and SWM relationship, greater RV basal bulging and higher LV conicity were associated with increased contractility. In order to address this discrepancy, RV basal bulging and LV conicity shape mode scores were correlated with patient-specific LV and RV EFs, providing insight into how these shape changes effect overall differences in global function rather than changes in global function along a specific component of SWM. Through this analysis, less RV basal bulging and lower LV conicity were correlated with higher LV and RV EF. Overall, these results suggest that while RV basal bulging and LV conicity may be surrogate measures for increased contractility in the RV posterior base and LV apex and base, the gain of function in these regions is overshadowed by the loss of function in other regions associated with shape itself. This

mechanism may explain why patients with rTOF that had less RV basal bulging and lower LV conicity had better outcomes [15].

4.2 Limitations

There were several simplifications that were employed in our FE analysis of biventricular mechanics. Material properties were assumed to be homogeneous throughout different regions of the heart including the entire RV and the entire LV, rather than including more specific regional heterogeneities that could be the result of scarring or fibrosis in areas with surgical incisions. The myocardial fiber architecture employed was also simplified using a rule-based approximation with a linear transmural gradient rather than using more realistic properties. This was primarily due to the lack of information on ventricular fiber architecture in a representative rTOF patient. Differences in hemodynamics between patients that might have also contributed to variation in shape and SWM were not considered due to the limited clinical availability of this data. Lastly, the FE models employed did not include boundary conditions representative of interactions with the pericardium, atria, and great vessels or include fluid-structure interactions.

5 Conclusions

In this study, statistical shape models were integrated with cardiac biomechanics models to further investigate the degree to which clinically significant shape markers are determinants of systolic function in a cohort of patients with rTOF. In FE simulations of systolic mechanics, variations in ED shape explained differences in SWM to varying degrees. Variation in RV apical dilation and LV dilation partially explained differences in SWM, while variation in RV basal bulging and LV conicity explained the opposite change in SWM. Specifically, greater RV apical dilation and less LV dilation were associated with increased RV basal and apical contractility and may be important determinants of improved function in rTOF. Overall, patients with rTOF may benefit from an atlas-based analysis of biventricular mechanics that can provide insight into mechanisms of pathophysiology and aid long-term clinical management.

Funding.

Funding was provided by National Institutes of Health R01HL121754 and American Heart Association 19AIML35120034. SG acknowledges National Institutes of Health NHLBI T32HL105373.

ADM and JHO are co-founders of, scientific advisors to, and equity holders in Insilicomed, Inc. ADM is also a co-founder of and scientific advisor to Vektor Medical, Inc. Some of their research grants have been identified for conflict-of-interest management. The authors are required to disclose these relationships in publications acknowledging the grant support; however, the findings reported in this study did not involve the companies in any way and have no relationship with the business activities or scientific interests of either company. The terms of this arrangement have been reviewed and approved by the University of California San Diego in accordance with its conflict-of-interest policies.

References

1. Diller GP, et al. : Left ventricular longitudinal function predicts life-threatening ventricular arrhythmia and death in adults with repaired tetralogy of fallot. Circulation 125(20), 2440–2446 (2012) [PubMed: 22496160]

2. Orwat S,et al. :Myocardial deformation parameters predict outcome in patients with repaired tetralogy of Fallot. Heart 102(3), 209–215 (2016) [PubMed: 26715570]
3. Kallhovd S, Sundnes J, Wall ST: Sensitivity of stress and strain calculations to passive material parameters in cardiac mechanical models using unloaded geometries. Comput. Methods Biomech. Biomed. Eng 1–12 (2019)
4. Aguado-Sierra J, et al. : Patient-specific modeling of dyssynchronous heart failure: a case study. Prog. Biophys. Mol. Biol 107(1), 147–155 (2011) [PubMed: 21763714]
5. Krishnamurthy A, et al. : Patient-Specific Models of Cardiac Biomechanics. J. Comput. Phys 244, 4–21 (2013) [PubMed: 23729839]
6. Medrano-Gracia P, et al. : Left ventricular shape variation in asymptomatic populations: the Multi-Ethnic Study of Atherosclerosis. J. Cardiovasc. Magn. Reson 16, 56 (2014) [PubMed: 25160814]
7. Farrar G, et al. : Atlas-Based Ventricular Shape Analysis for Understanding Congenital Heart Disease. Prog. Pediatr. Cardiol 43, 61–69 (2016) [PubMed: 28082823]
8. Gilbert K, et al. : Independent left ventricular morphometric atlases show consistent relationships with cardiovascular risk factors: A UK Biobank Study. Sci. Rep 9(1), 1130 (2019) [PubMed: 30718635]
9. Mauger C, et al. : Right ventricular shape and function: cardiovascular magnetic resonance reference morphology and biventricular risk factor morphometrics in UK Biobank. J. Cardiovasc. Magn. Reson 21(1), 41 (2019) [PubMed: 31315625]
10. Mauger CA, et al. : Right-left ventricular shape variations in tetralogy of Fallot: associations with pulmonary regurgitation. J. Cardiovasc. Magn. Reson 23(1), 105 (2021) [PubMed: 34615541]
11. Geva T: Repaired tetralogy of Fallot: the roles of cardiovascular magnetic resonance in evaluating pathophysiology and for pulmonary valve replacement decision support. J. Cardiovasc. Magn. Reson 13, 9 (2011) [PubMed: 21251297]
12. Broberg CS, et al. : Prevalence of left ventricular systolic dysfunction in adults with repaired tetralogy of fallot. Am. J. Cardiol 107(8), 1215–1220 (2011) [PubMed: 21349477]
13. Valente AM, et al. : Contemporary predictors of death and sustained ventricular tachycardia in patients with repaired tetralogy of Fallot enrolled in the INDICATOR cohort. Heart 100(3), 247–253 (2014) [PubMed: 24179163]
14. Probst J, et al. : Prevention of sudden cardiac death in patients with Tetralogy of Fallot: Risk assessment and long term outcome. Int. J. Cardiol 269, 91–96 (2018) [PubMed: 29980366]
15. Govil S, et al. , Biventricular Shape Modes Discriminate Pulmonary Valve Replacement in Tetralogy of Fallot Better Than Imaging Indices. Sci. Rep (2022). (In Review)
16. Fonseca CG, et al. : The Cardiac Atlas Project—an imaging database for computational modeling and statistical atlases of the heart. Bioinformatics 27(16), 2288–2295 (2011) [PubMed: 21737439]
17. Holzapfel GA, Ogden RW: Constitutive modelling of passive myocardium: a structurally based framework for material characterization. Philos. Trans. A Math. Phys. Eng. Sci 2009(367), 3445–3475 (1902)
18. Krishnamurthy A, et al. : Left Ventricular Diastolic and Systolic Material Property Estimation from Image Data: LVM echanics Challenge. Stat. Atlases. Comput. Models Heart 8896,63–73 (2015) [PubMed: 25729778]
19. Doste R, et al. : A rule-based method to model myocardial fiber orientation in cardiac biventricular geometries with outflow tracts. Int. J. Numer. Method. Biomed. Eng 35(4), e3185 (2019) [PubMed: 30721579]

A

SWM Mode	1	2	3	4	5	6	7	8	9	10
Variance Explained (%)	15	14	10	7	5	4	4	4	3	2

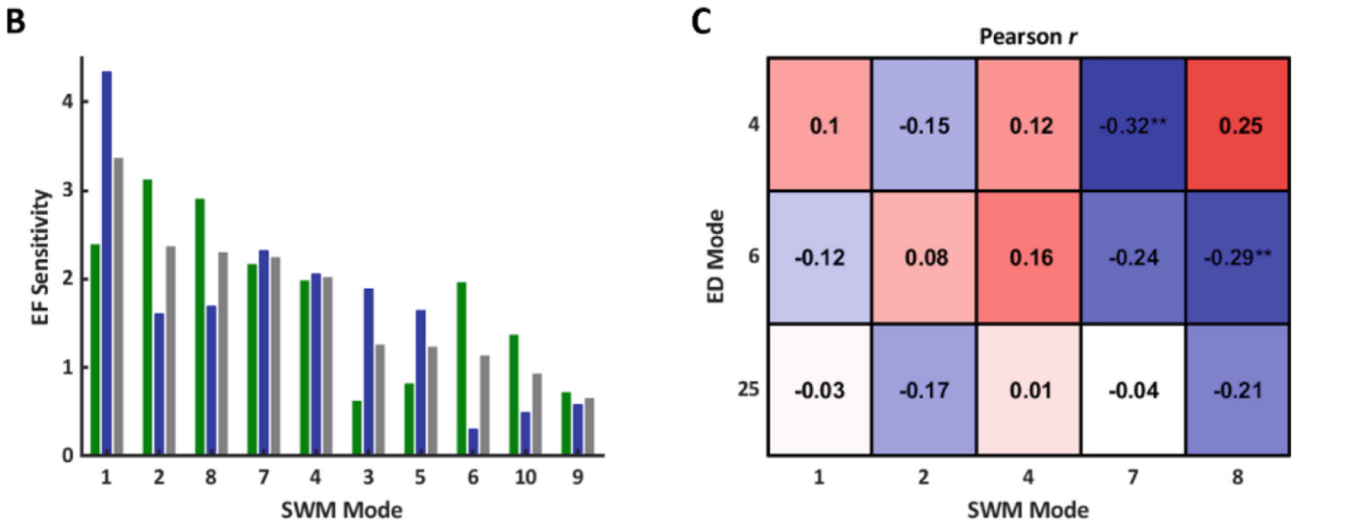

Fig. 1.

A) Variance explained (%) per SWM mode. B) Magnitude of the sensitivity of LV EF (green), RV EF (blue), and combined LV/RV EF (grey) to variations in SWM modes (pp/SD). SWM modes were ranked from greatest to least effect on combined LV/RV EF. C) Correlations between clinically significant ED shape modes and SWM modes that had the greatest effect on combined LV/RV EF. Symbols indicate statistical significance (**$p < 0.01$).

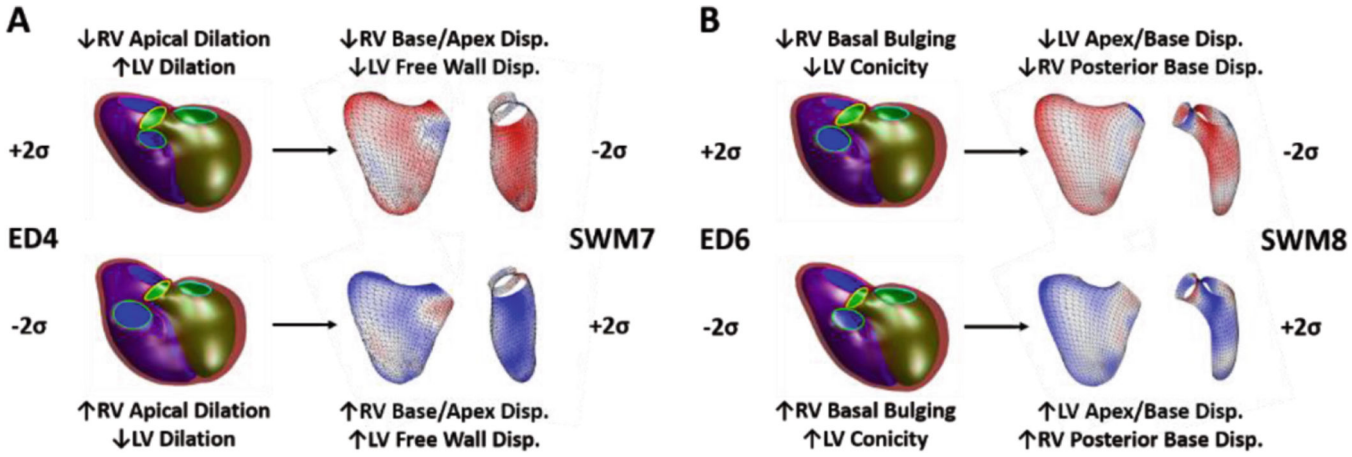

Fig. 2.

Summary morphological characteristics for associations between ED shape and SWM, (A) ED4 ∝ SWM7 and (B) ED6 ∝ SWM8. For ED shape modes, the LV endocardial surface, RV endocardial surface, and epicardial surface are shown in green, blue, and maroon, respectively, and the mitral, tricuspid, aortic, and pulmonary valves are shown in cyan, pink, yellow, and green, respectively. For SWM modes, the LV and RV free walls are shown and are colored based on the systolic displacement relative to the mean, inward (blue) and outward (red).

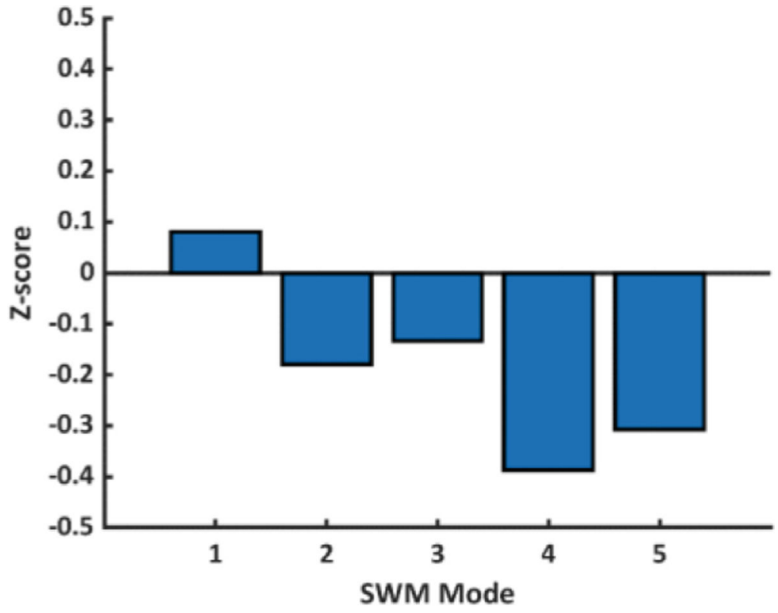

Fig. 3.

Difference between mean FE-computed model (blue bar) and atlas model (black line) SWM Z-scores. (Color figure online)

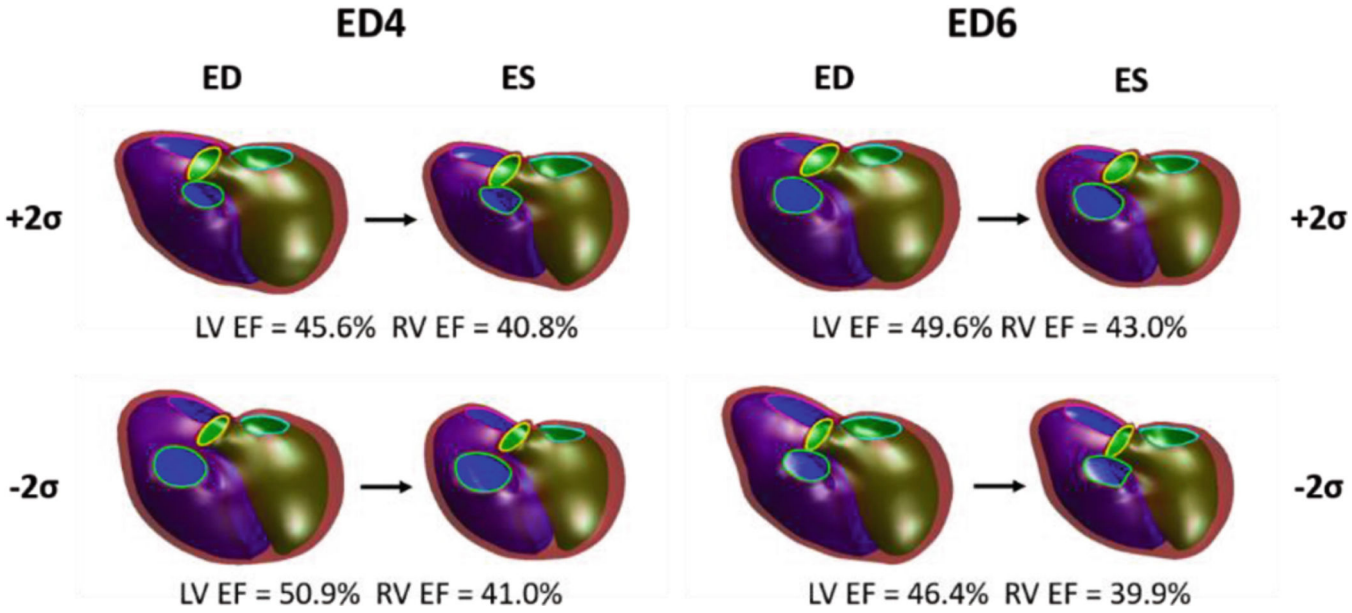

Fig. 4.

FE-computedEDshapeperturbationswithcorrespondingdeformedESshapes.Computed LV and RV EFs for each shape perturbation are also shown. For all models, the LV endocardial surface, RV endocardial surface, and epicardial surface are shown in green, blue, and maroon, respectively, and the mitral, tricuspid, aortic, and pulmonary valves are shown in cyan, pink, yellow, and green, respectively.

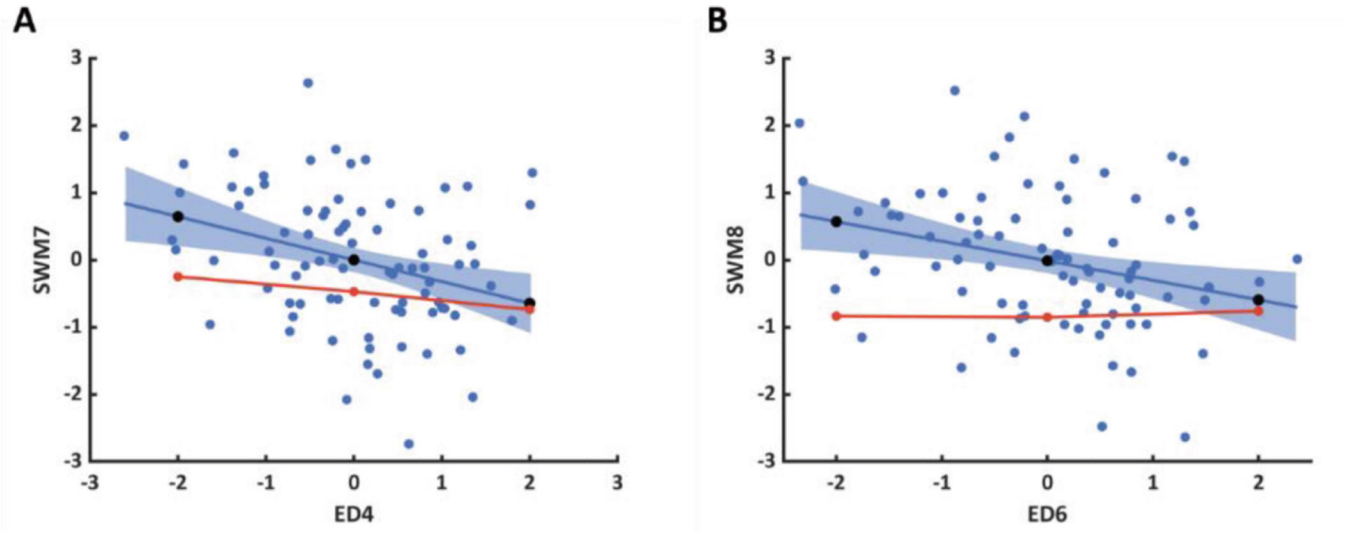

Fig. 5.

Comparison of predicted (black circles) and FE-computed (red line and circles) SWM Z-scores for shape perturbations along (A) ED4 ∝ SWM7 and (B) ED6 ∝ SWM8 using mean material properties. Significant ED shape mode and SWM mode correlations from patient data (blue circles) are represented as linear regression models with the fit (blueline) and 95% confidence intervals (blue shaded area).

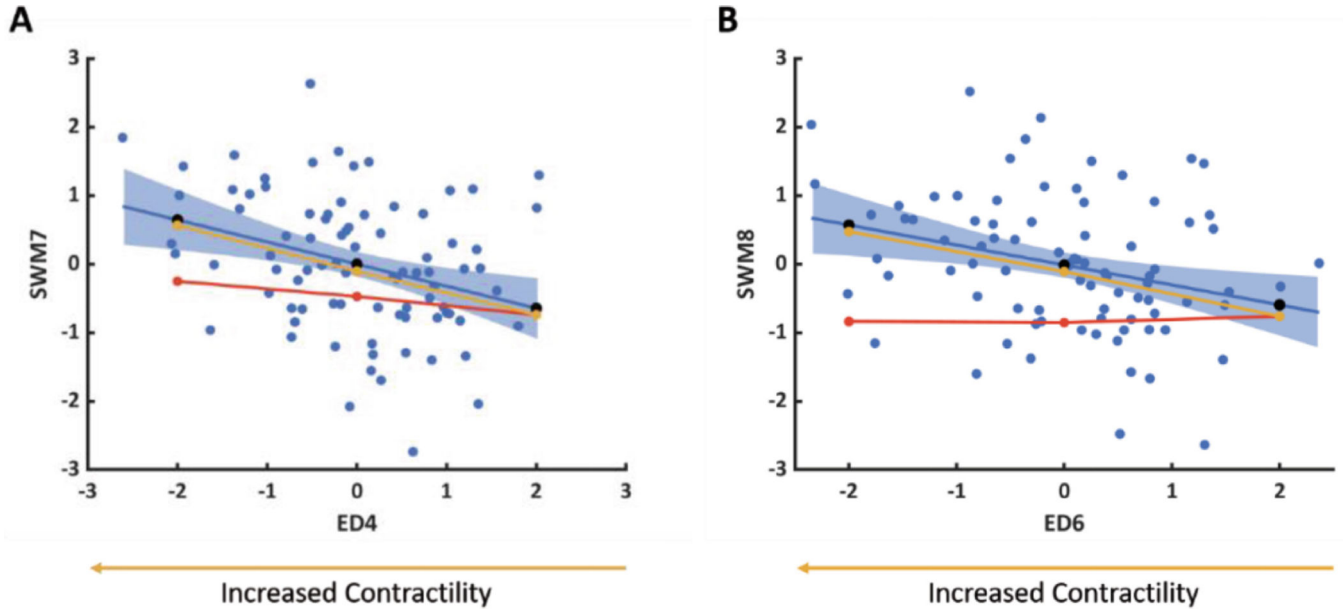

Fig. 6.

FE-computed changes in SWM Z-scores for shape perturbations along (A) ED4 ∝ SWM7 and (B) ED6 ∝ SWM8 with altered contractility (yellow line and circles) overlaid on Fig. 5. The direction of ED shape variation associated with increased contractility is also shown.

Table 1.

Estimated mean passive material properties.

Region	*a* (kPa)	*af* (kPa)	*b* (−)	*bf* (−)
LV	1.197	0.8925	9.726	15.779
RV	2.394	1.785	9.726	15.779
Base	11.97	8.925	9.726	15.779

Table 2.

Comparison of mean FE-computed model and atlas model volumes and EFs.

Measure	Atlas Model	FE-Computed Model
LV EDV (mL)	78.3	77.9
LV ESV (mL)	38.8	39.7
RV EDV (mL)	153.4	153.3
RV ESV (mL)	89.2	87.9
LV EF (%)	50.5	49.0
RV EF (%)	41.9	42.7